Electronic Supplementary Information for

UNAM-1: A robust Cu^{I} and Cu^{II} containing 3D-hydrogen-bonded framework with permanent porosity and reversible SO$_2$ sorption

Ricardo Domínguez-González,[a,b] Irán Rojas-León,[b] Eva Martínez-Ahumada,[c] Diego Martínez-Otero,[a,b] Hugo A. Lara-García,[d] Jorge Balmaseda-Era,[c] Ilich A. Ibarra,[c] Edmundo G. Percástegui[a,b] and Vojtech Jancik[a,b,*]

- [a.] Universidad Nacional Autónoma de México, Instituto de Química, Ciudad Universitaria, Ciudad de México, 04510, Mexico. E-mail: vjancik@unam.mx
- [b.] Centro Conjunto de Investigación en Química Sustentable UAEM-UNAM, Carretera Toluca-Atlacomulco km 14.5, Toluca, Estado de México, 50200, México.
- [c.] Laboratorio de Fisicoquímica y Reactividad de Superficies (LaFReS), Instituto de Investigaciones en Materiales, Universidad Nacional Autónoma de México, Circuito Exterior s/n, CU, Del Coyoacán, 04510, México D.F., México.
- [d.] Instituto de Física, Universidad Nacional Autónoma de México, Circuito de la Investigación científica s/n, CU, Del. Coyoacán, 04510, Ciudad de México, Mexico.

Index

Experimental

General methods

Copper(II) acetate dihydrate was synthesized from Sigma-Aldrich (Merk©) copper(II) sulfate pentahydrate and purified by recrystallization in water. 1,2,3-triazole-4,5-dicarboxylic acid (**H₃L**) was synthesized according to reference (1). DMF 99% was used without any previous treatment. N,N'-dimethylaniline was purchased from Sigma-Aldrich (Merk©) and used as received.

Elemental analyses (C, H, N) were performed on an Elementar MicroVario Cube analyzer. Melting points were measured in glass capillary tubes on a Büchi B-540 melting point apparatus. FT-IR spectra were recorded on a Bruker ALPHA FTIR spectrometer using the ATR technique with a diamond window in the range of $\tilde{v}$ 400–4000 cm⁻¹. TGA measurements were carried on a Netzsch STA 449 F3 Jupiter with a heating rate of 10 °C/min from room temperature to 450 °C under nitrogen atmosphere. Powder X-ray diffraction patterns were measured on a Bruker D8 Advance X-ray diffractometer equipped with a LynxEye detector using CuK_α radiation (λ = 1.5406 Å; monochromator: germanium) in a range 2-theta of 4–60° with a step of 0.01°. The UV-visible spectra were recorded on a Thermo Scientific Genesys 10 spectrophotometer in range of 10000–25000 cm⁻¹. The paramagnetic resonance spectrum was measured in x-band in an EPR spectrometer Jeol, JES-TE300, in solid at room temperature. HRMS spectrum was measured on a Bruker micro-TOF II spectrometer using ESI ionization.

Synthesis of UNAM-1
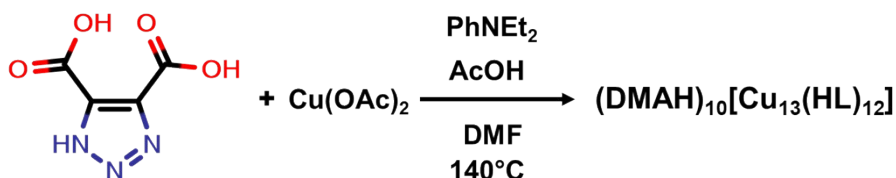
(DMAH)₁₀[Cu₁₃(HL)₁₂] **(UNAM-1)**. A mixture of Cu(OAc)₂·H₂O (0.0119 g, 0.06 mmol), **H₃L** (0.0116 g, 0.06 mmol),[1] DMF (2.0 mL), N,N'-dimethylaniline (0.0119 g, 0.08 mmol) and acetic acid (0.0048 g, 0.08 mmol) was heated at 140 °C for 72 h in a 4 mL borosilicate glass vial. After this time, the reaction mixture was cooled to room temperature at a rate of 0.6 °C min⁻¹, the crystalline product was washed thoroughly with DMF and dried at 70 °C under vacumm yielding purple cubic shape crystals, (0.0107 g). Yield: 68 % (DMAH)₁₀[Cu₁₃(HL)₁₂]·7.5DMF·7H₂O, C₉₀.₅H₁₅₈.₅N₅₃.₅O₆₂.₅Cu₁₃. Elemental Analysis (%) Calc. C 28.44%, H 4.18%, N 19.61%; Found: C 28.72%, H 4.02%, N 19.35%. Decomp. point 360 °C. IR-Spectroscopy: 3433(w), 3052(w), 2799(w), 2481(w), 1657(s), 1578(s), 1504(s), 1465(s), 1367(s), 1287(m), 1254(m), 1208(m), 1156(m), 1095(m), 1060(m), 1020(m), 973(m), 837(m), 782(m), 699(w), 663(m), 534(m), 421(w) (See Fig. S1 for full IR spectrum).
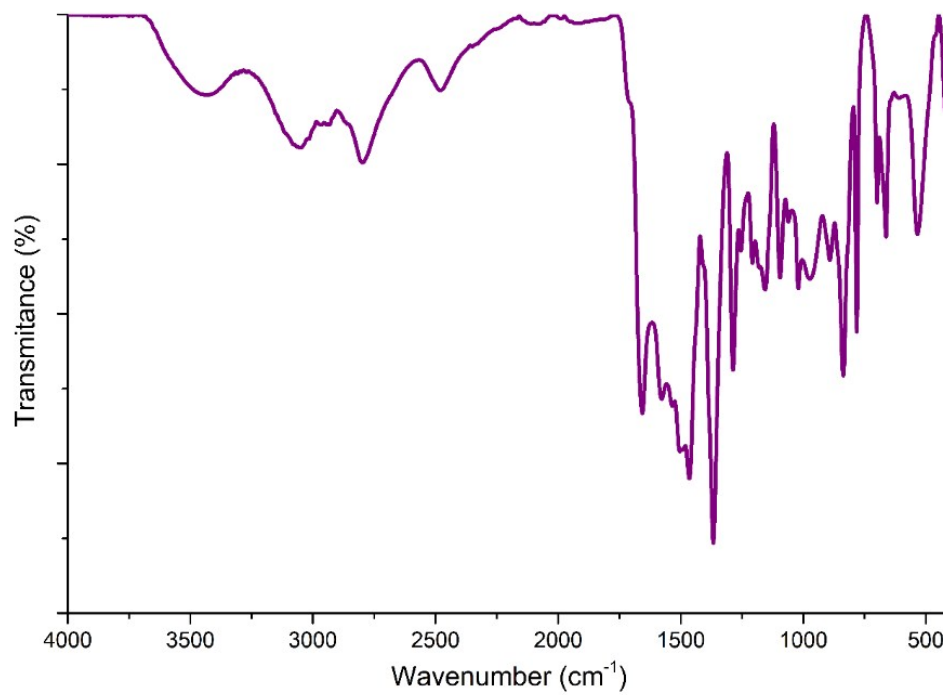
Infrared spectroscopy

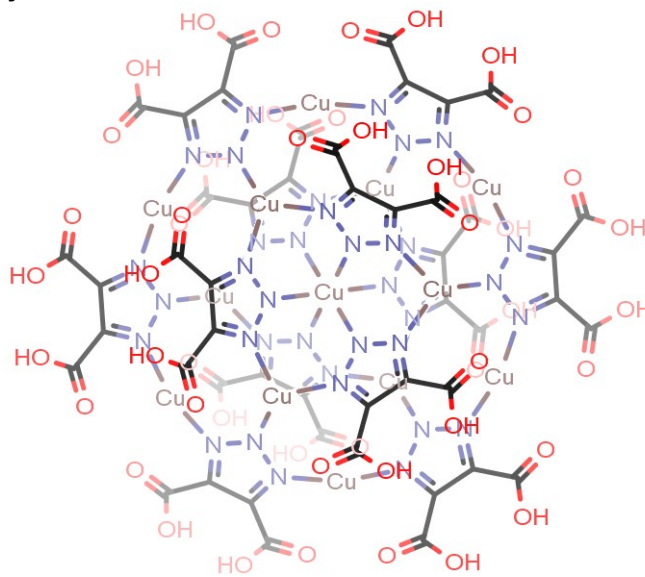**Figure S1**. The ATR-FT-IR spectrum of **UNAM-1**.

Mass spectrometry

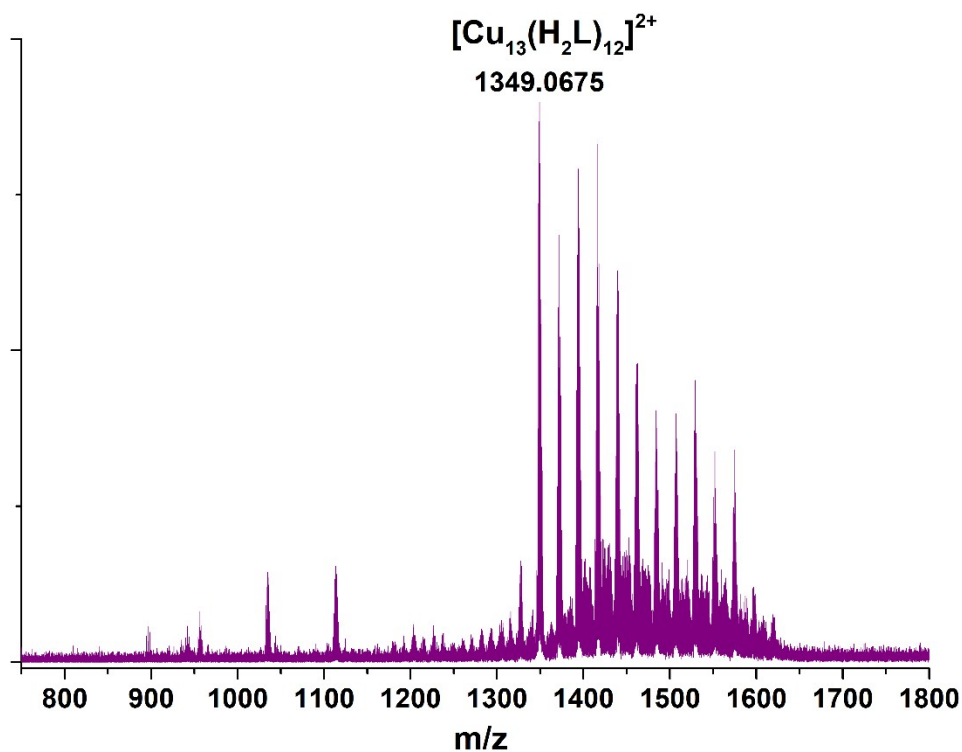**Figure S2**. The $[Cu_{13}(H_2L)_{12}]^{2+}$ ion observed in the mass spectrum of **UNAM-1**.
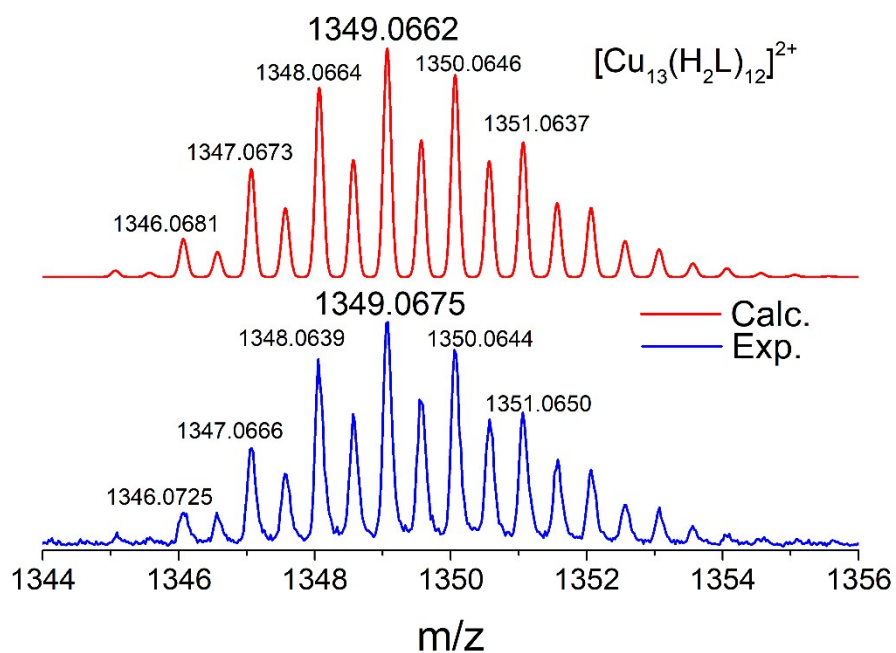
Figure S3. ESI-TOF(+) mass spectrum of **UNAM-1**.

Figure S4. Calculated (above) vs. experimental isotopic patterns (below) for $[Cu_{13}(H_2L)_{12}]^{2+}$. Formula: $C_{48}H_{24}N_{36}O_{48}Cu_{13}$; Error = 0.96 ppm.
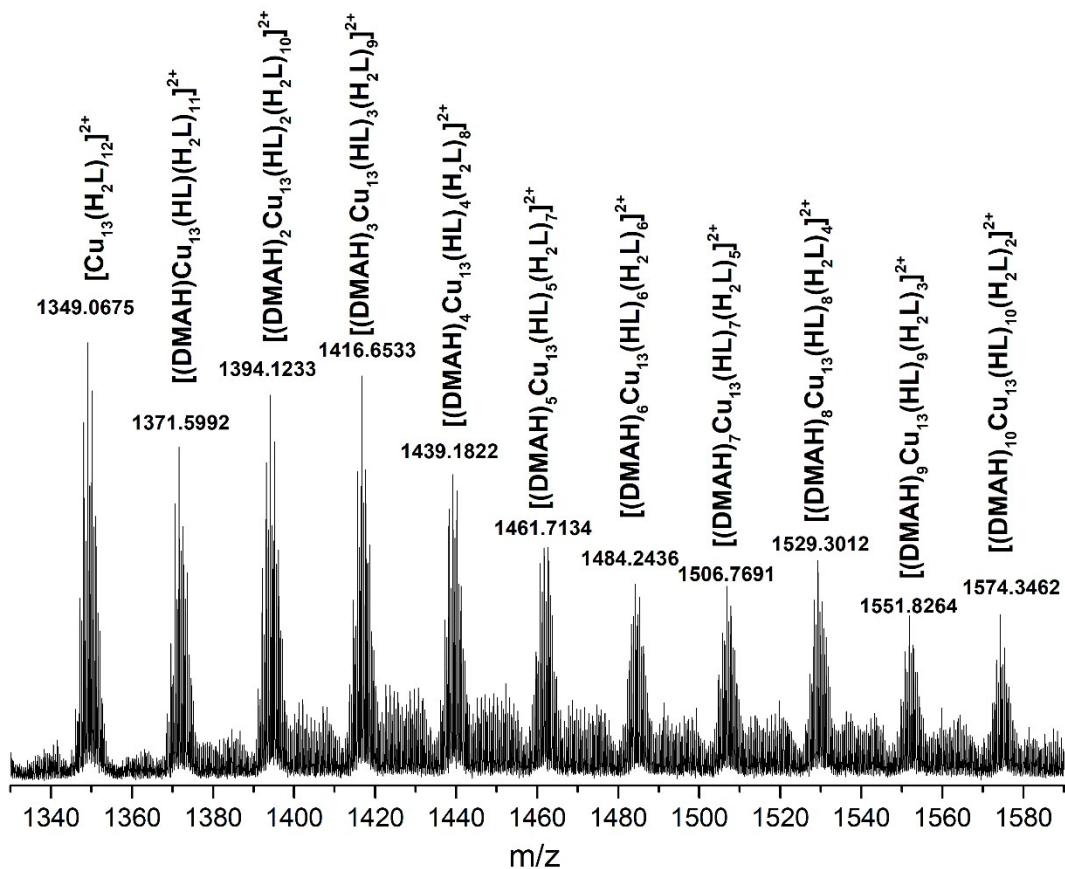
Figure S5. Ionic species found in the mass spectrum ESI-TOF(+) of **UNAM-1**.

Table S1. Different ionic species identified in the ESI-TOF(+) mass spectrum of **UNAM-1**.

| Formula moiety	Formula sum	Calculated	Experimental	Error (ppm)
$[Cu_{13}H_{12}(H_2L)_{12}]^{2+}$	$C_{48}H_{24}N_{36}O_{48}Cu_{13}$	1349.0662	1349.0675	0.96
$[(DMAH)Cu_{13}(HL)(H_2L)_{11}]^{2+}$	$C_{50}H_{31}N_{37}O_{48}Cu_{13}$	1371.5951	1371.5992	2.99
$[(DMAH)_2Cu_{13}(HL)_2(H_2L)_{10}]^{2+}$	$C_{52}H_{38}N_{38}O_{48}Cu_{13}$	1394.1241	1394.1233	−0.57
$[(DMAH)_3Cu_{13}(HL)_3(H_2L)_9]^{2+}$	$C_{54}H_{45}N_{39}O_{48}Cu_{13}$	1416.6531	1416.6533	0.14
$[(DMAH)_4Cu_{13}(HL)_4(H_2L)_8]^{2+}$	$C_{56}H_{52}N_{40}O_{48}Cu_{13}$	1439.1820	1439.1822	0.14
$[(DMAH)_5Cu_{13}(HL)_5(H_2L)_7]^{2+}$	$C_{58}H_{59}N_{41}O_{48}Cu_{13}$	1461.7110	1461.7134	1.64
$[(DMAH)_6Cu_{13}(HL)_6(H_2L)_6]^{2+}$	$C_{60}H_{66}N_{42}O_{48}Cu_{13}$	1484.2400	1484.2436	2.43
$[(DMAH)_7Cu_{13}(HL)_7(H_2L)_5]^{2+}$	$C_{62}H_{73}N_{43}O_{48}Cu_{13}$	1506.7689	1506.7691	0.13
$[(DMAH)_8Cu_{13}(HL)_8(H_2L)_4]^{2+}$	$C_{64}H_{80}N_{44}O_{48}Cu_{13}$	1529.2979	1529.3012	2.16
$[(DMAH)_9Cu_{13}(HL)_9(H_2L)_3]^{2+}$	$C_{66}H_{87}N_{45}O_{48}Cu_{13}$	1551.8268	1551.8264	−0.26
$[(DMAH)_{10}Cu_{13}(HL)_{10}(H_2L)_2]^{2+}$	$C_{68}H_{94}N_{46}O_{48}Cu_{13}$	1574.3558	1574.3462	−6.10

UV-Vis Spectroscopy
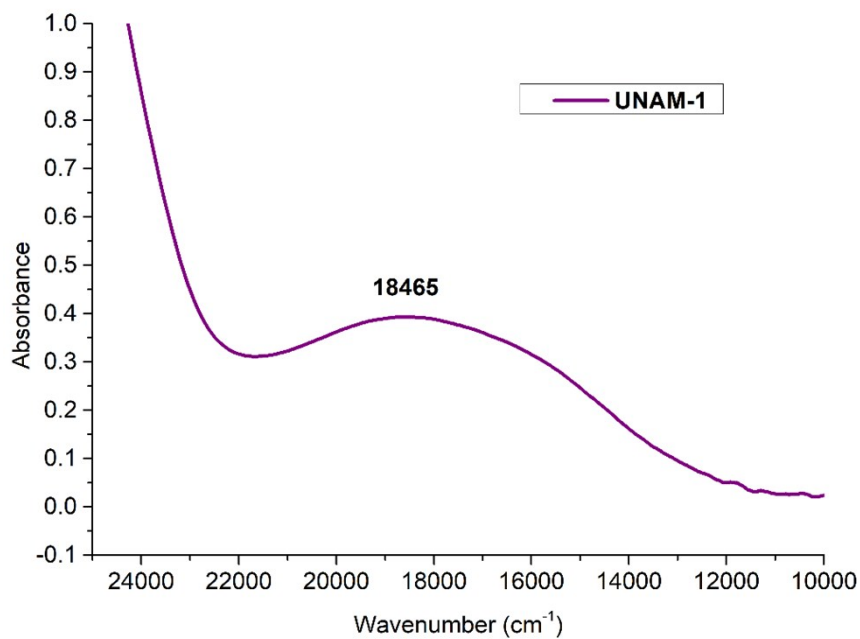
Figure S6. The UV-Vis spectrum of **UNAM-1**. A single transition $^2E_g \leftarrow {}^2T_g$ for the central octahedral Cu^{II} ion can be seen at 18,465 cm^{-1}.
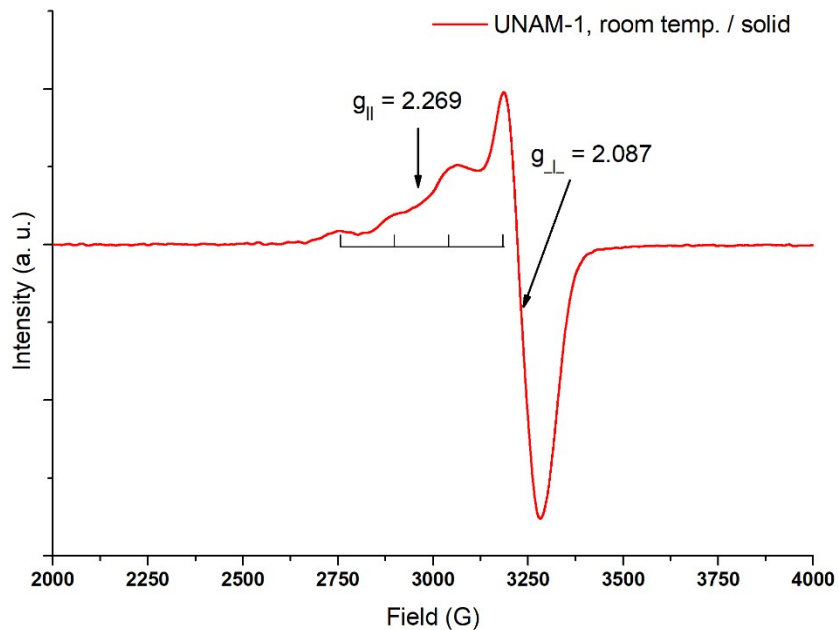
Electron paramagnetic resonance

Figure S7. X-band EPR spectrum of **UNAM-1** in solid state at room temperature.

X-ray structure determination

Table S2. Data collection and refinement details for **UNAM-1**

	UNAM-1
Empirical formula	$C_{68}H_{92}Cu_{13}N_{46}O_{48}$ + solvent
Moiety formula	$C_{48}H_{12}Cu_{13}N_{36}O_{48}$, $10(C_2H_8N)$ + solvent
Molecular weight	3147.89
Color	Purple
Crystal system	Cubic
Space group	$Im\bar{3}m$
Temp (K)	296(2)
λ, (Å)	1.54178
a (Å)	32.3206(2)
b (Å)	32.3206(2)
c (Å)	32.3206(2)
α (deg)	90
β (deg)	90
γ (deg)	90
V (Å^3)	33762.8(6)
Z	8
ρ_{calc} (Mg m^{-3})	1.239
μ (mm^{-1})	2.366
$F(000)$	12664
Crystal size (mm)	0.282 x 0.266 x 0.256
θ range (deg)	1.933–68.324
Index ranges	$-32 \leq h \leq 38$
	$-38 \leq k \leq 29$
	$-30 \leq l \leq 36$
Reflections collected	48512
Independent reflections ($R_{int.}$)	2953 (0.0493)
data/restrains/parameters	2953 / 448 / 290
GoF on F^2	1.039
R_1,[a] wR_2[b] ($I > 2\sigma(I)$)	0.0592, 0.1831
R_1,[a] wR_2[b] (all data)	0.0659, 0.1957
Voids in the unit cell (volume in Å^3 / electrons):	9292 / 2244
Largest diff. peak / hole (e Å^{-3})	0.629 / −0.489
CCDC	1941697

[a] $R_1 = \sum ||F_o| - |F_c||/\sum|F_o|$. [b] $wR_2 = [\sum w(F_o^2 - F_c^2)^2/\sum(F_o^2)^2]^{1/2}$.

Single crystals of UNAM-1 was mounted inside a capillary and was covered with a drop of the mother liquor and placed inside a Bruker APEX DUO diffractometer equipped with an Apex II CCD detector using CuK$_\alpha$ (λ = 1.54178 Å) Incoatec IµS microsource and multilayer optic monochromator. Frames were collected using omega scans and integrated with SAINT.[2] Multi-scan absorption correction (SADABS) was applied.[2] The structures were solved by direct methods (SHELXT)[3] and refined using full-matrix least-squares on F^2 with SHELXL[4] within the ShelXle GUI.[5] Weighted R factors, wR, and all goodness-of-fit indicators are based on F^2. All non-

hydrogen atoms were refined anisotropically. The hydrogen atoms of the C–H, N–H and O–H bonds were placed in idealized positions. The disordered groups and cations were refined using geometry (SAME/SADI, DFIX, and FLAT) and U_{ij} restraints (SIMU, RIGU, ISOR) implemented in SHELXL.[4] The molecular graphics were prepared using Diamond,[6] Mercury,[7] POV-RAY,[8] Corel Draw X7[9] and GIMP.[10] CCDC-1941697 (**UNAM-1**) contains the supplementary crystallographic data for this paper. These data can be obtained free of charge via http:/www.ccdc.cam.ac.uk/const/retrieving.html (or from the Cambridge Crystallographic Data Centre, 12 Union Road, Cambridge CB21EZ, UK; fax: (+44)1223-336-033; or deposit@ccdc.cam.ac.uk).

Table S3. Selected bond lengths [Å] and angles [°] for **UNAM-1**

Cu3–N1	2.157 (3)
Cu1–N2	1.980 (3)
Cu1–N4	1921 (9)
Cu2–N3	1.93(3)
Cu2–N3	1.93(3)
N1–Cu3–N1a	90.07 (13)
N2–Cu1–N2b	99.01 (12)
N2–Cu1–N4	129.8 (3)
N3–Cu2–N3	43.45 (19)

a: z, x, y; **b**: x, z, y

Table S4. Hydrogen bonds within the crystalline structure of **UNAM-1**

Atoms	D···A (Å)	H···A (Å)	Ang. D–H···A (°)
N1Bh–H1B1h···O1	2.787 (14)	1.97	153
N1Db–H1D2b···O3	2.868 (14)	1.99	169
N1Dg–H1D2g···O5	2.809 (10)	1.99	152
O2–H2···O2f	2.446 (6)	1.64	168
O3–H2···O5	2.568 (8)	1.79	158

b: x, z, y; **f**: z, y, x; **g**: x, y, –z; **h**: 0.5–y, 0.5–x, 0.5–z;
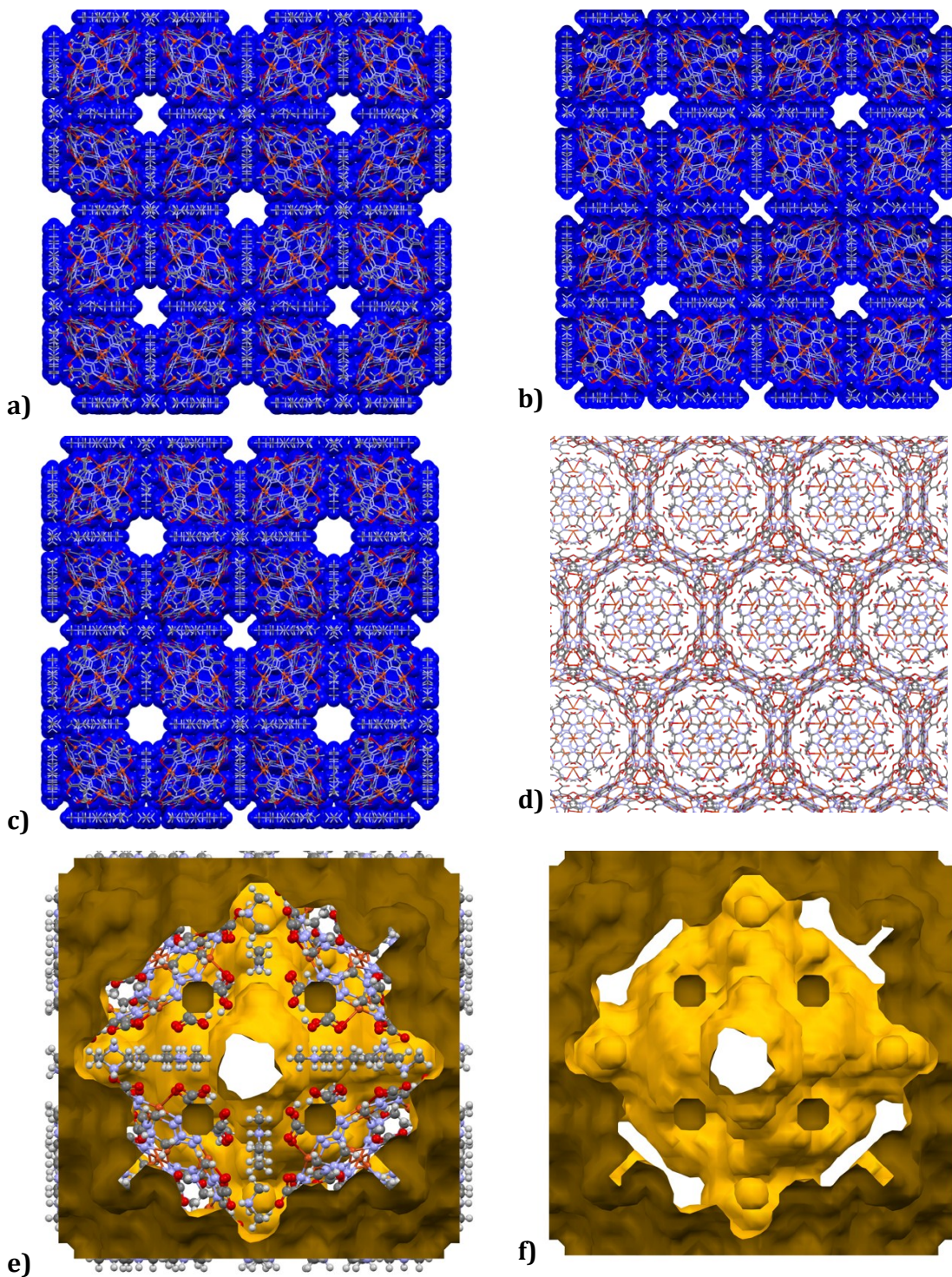
Figure S8. (a–c) Space-filling representation of the resulting framework with the location of the channel openings. For these figures, the structure of UNAM-1 was expanded to P1 and the positions of the disordered dimethylammonium cations were selected (from the refined positions) so all possible channel windows would be visible within the a, b, c sides of the unit cell. d) 111 direction view on the packing in UNAM-1. (e-f) Size and shape of the voids present in the centre and corners of the unit cells with (e) and without (f) the ions. Outside (yellow) and inside (brown) surface of the cavity.
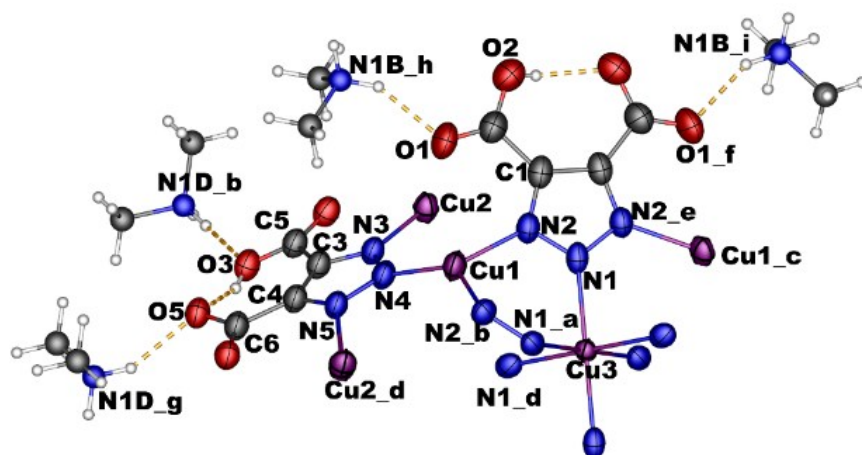
Figure S9. Asymmetric unit of **UNAM-1**. Thermal ellipsoids for the main anion are at 50% probability. Dimethylammonium ctions are represented as ball and sticks. Hydrogen bonds are depicted as dashed yellow bonds.
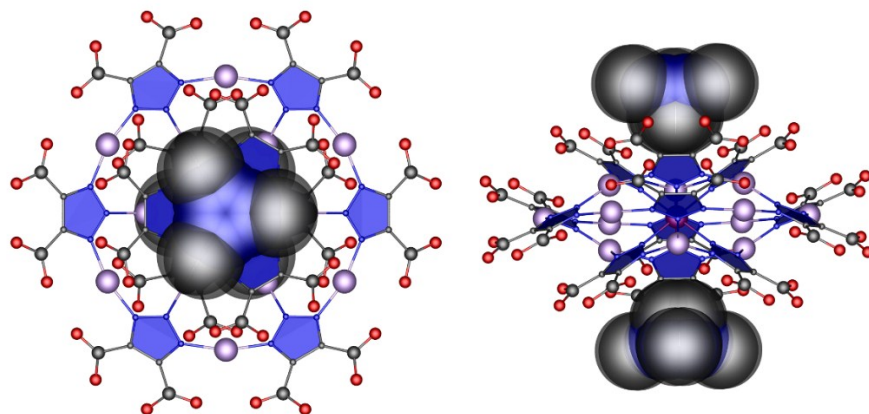

Figure S10. DMAH ions with 0.5 occupancy hosted in the axial positions of the $[Cu_{13}(HL)_{12}]^{10-}$ anion of **UNAM-1**.

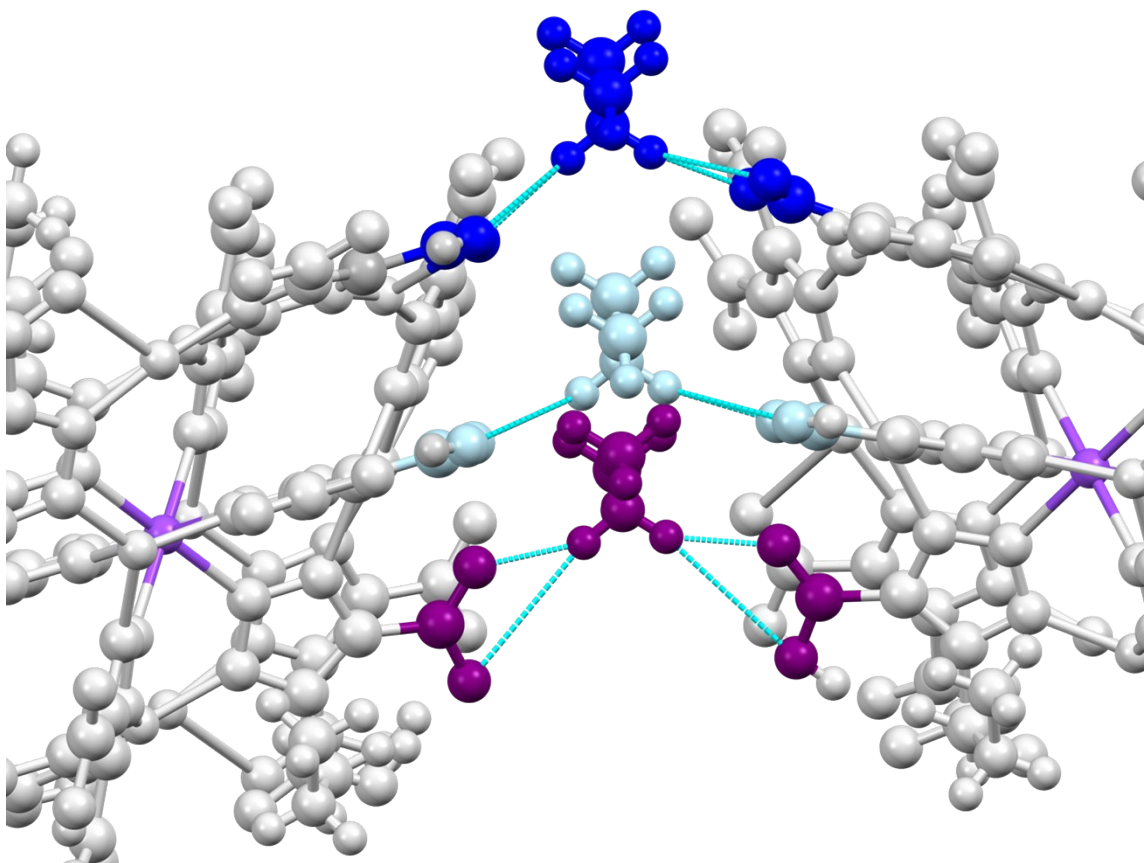**Figure S11.** Example of a hydrogen bonds between two $[Cu_{13}(HL)_{12}]^{10-}$ anions and dimethylammonium cations in **UNAM-1**.
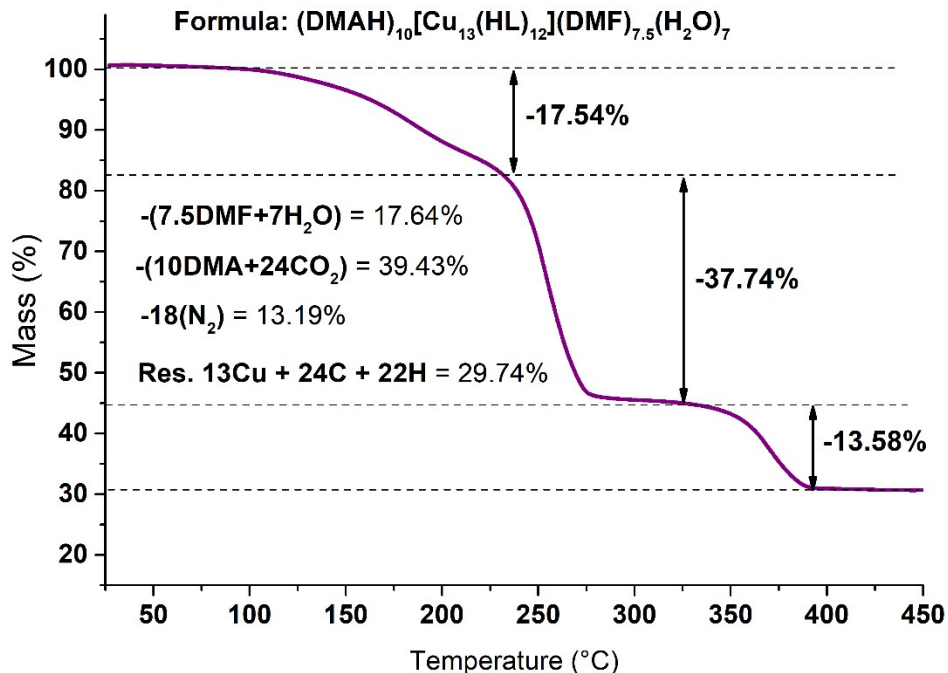
Thermogravimetric analysis

Formula: $(DMAH)_{10}[Cu_{13}(HL)_{12}](DMF)_{7.5}(H_2O)_7$

-17.54%

-37.74%

-13.58%

$-(7.5DMF+7H_2O) = 17.64\%$

$-(10DMA+24CO_2) = 39.43\%$

$-18(N_2) = 13.19\%$

Res. $13Cu + 24C + 22H = 29.74\%$

Figure S12. Thermogram of **UNAM-1**.

BET and Sorption experiments

Microstructural features were obtained from N_2 adsorption/desorption isotherm at $-196\,°C$ in a Quantachrome Autosorb MP-1 equipment. Before the measurement, the sample (0.050 g) was degasified under vacuum at $70\,°C$ during 1 h. The Brunauer–Emmett–Teller (BET) method was used for calculation of the specific surface area.

BET SSA = 522 $m^2\,g^{-1}$
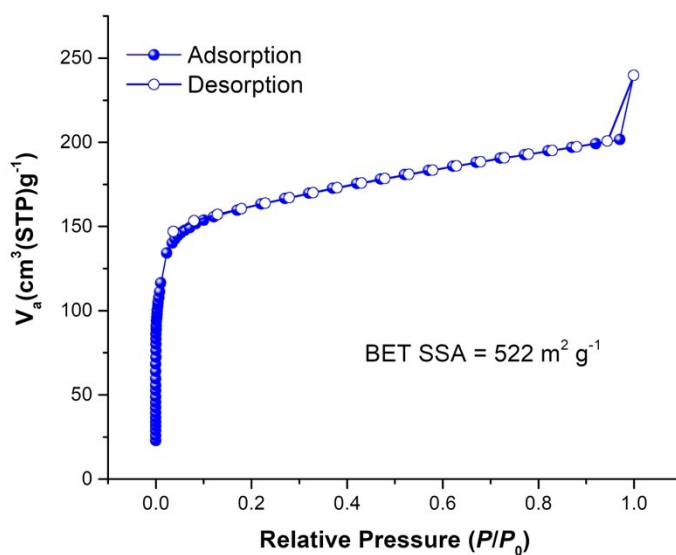
Figure S13. N_2 sorption isotherm of **UNAM-1** activated at 70 °C and collected at 77 K.

Area = 522 m²/g
Slope = 7.022E+00
Y Intercept = -0.13182
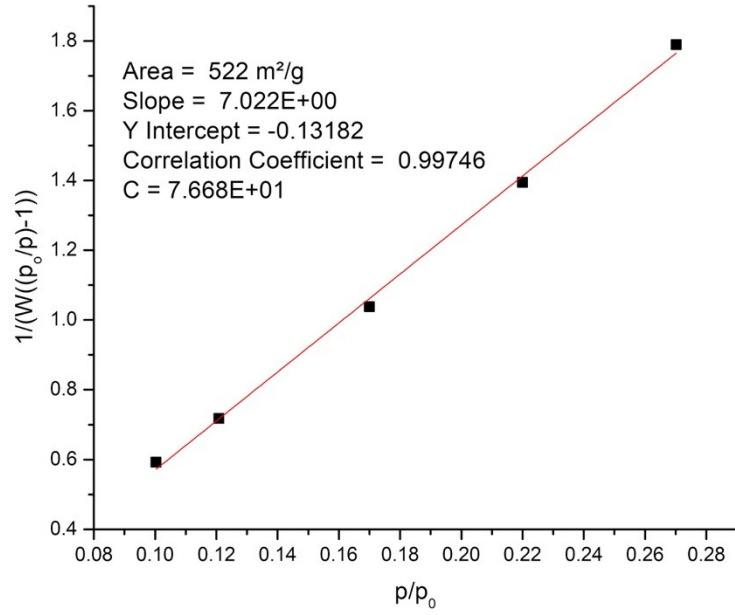Correlation Coefficient = 0.99746
C = 7.668E+01

Figure S14. Plot of the linear region for the BET equation (from the N_2 adsorption isotherm of **UNAM-1** activated at 70 °C).
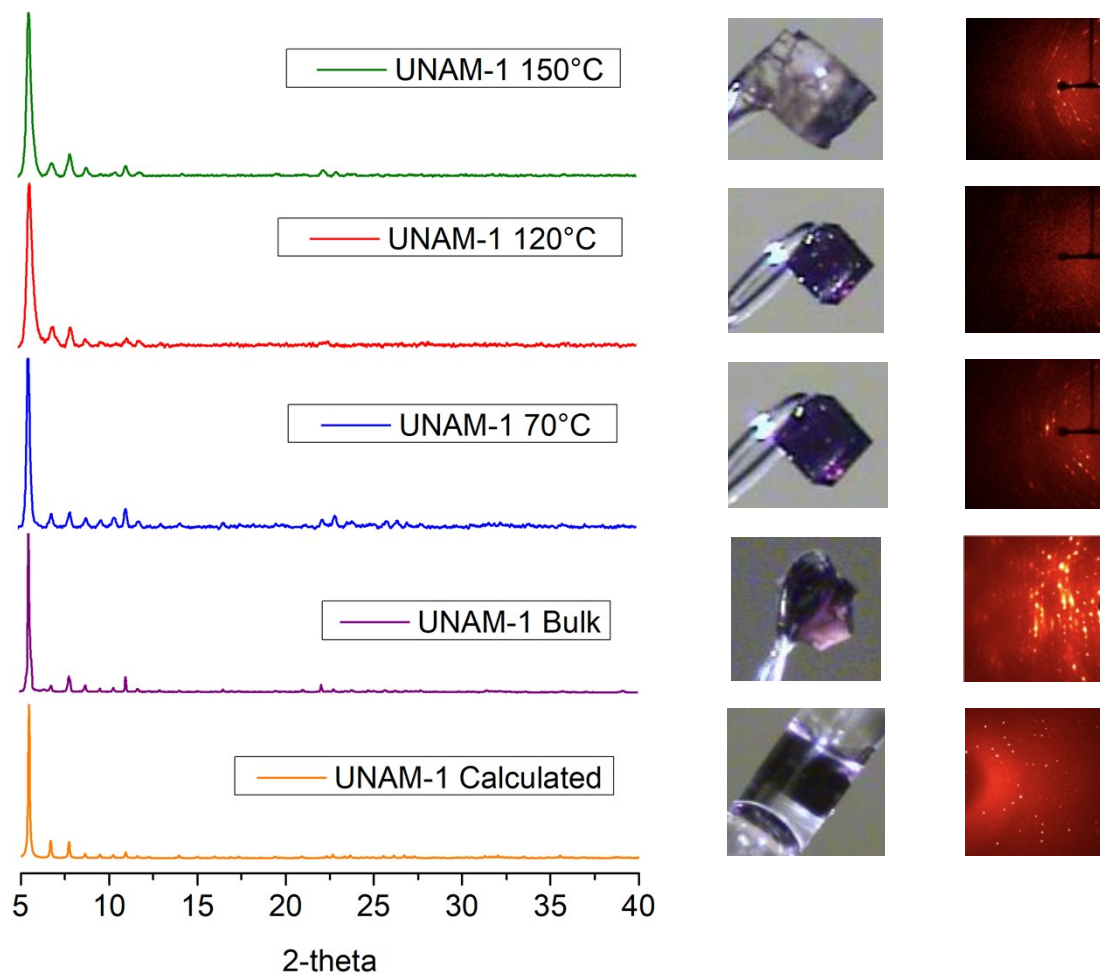
Figure S15. The effect of the activation temperature on the integrity of **UNAM-1** crystals. Left column Powder DRX, middle column: photo of a crystal, right column: 2D diffraction pattern of the crystal.

At 70 ^{o}C, the crystal maintains its integrity and a diffraction power. At 120 ^{o}C, the crystal as whole maintains integrity, but looses internal periodicity as evidenced by 2D single crystal X-ray diffraction and lower intensity of the powder X-Ray diffraction. At 150 ^{o}C the crystal shows severe cracks but regains diffractive power in both powder and monocrystal X-Ray diffraction. The powder diffractograms at 70 and 150 ^{o}C point to a phase retention, and the cracking of the crystal is most probably the result of the expansion of the DMF vapour pressure inside the crystal at 150 ^{o}C and the small window size of the pore that does not allow an efficient release of the solvent from the crystal.

For SO$_2$ sorption, the sample was activated at 70 °C under vacuum (1·10^{-6} bar) for 60 min. SO$_2$ adsorption was carried out at 298 K up to 1 bar in a Dynamic Gravimetric Gas/Vapour Sorption Analyser, DVS vacuum (Surface Measurement Systems Ltd).
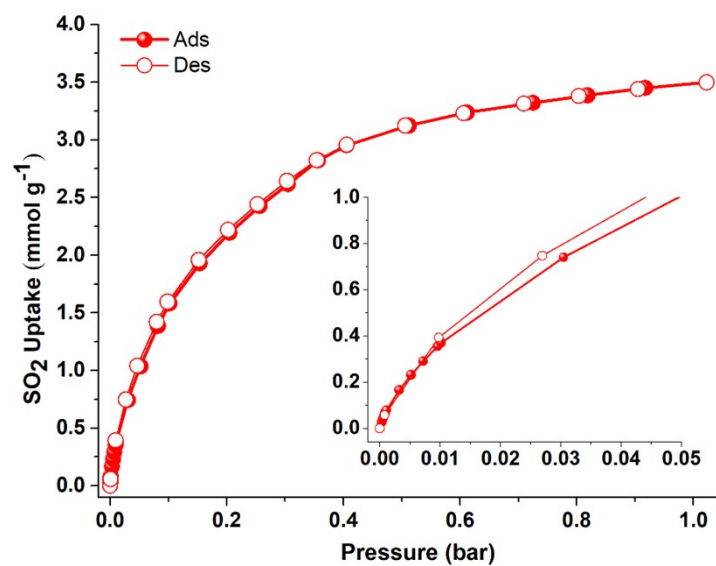

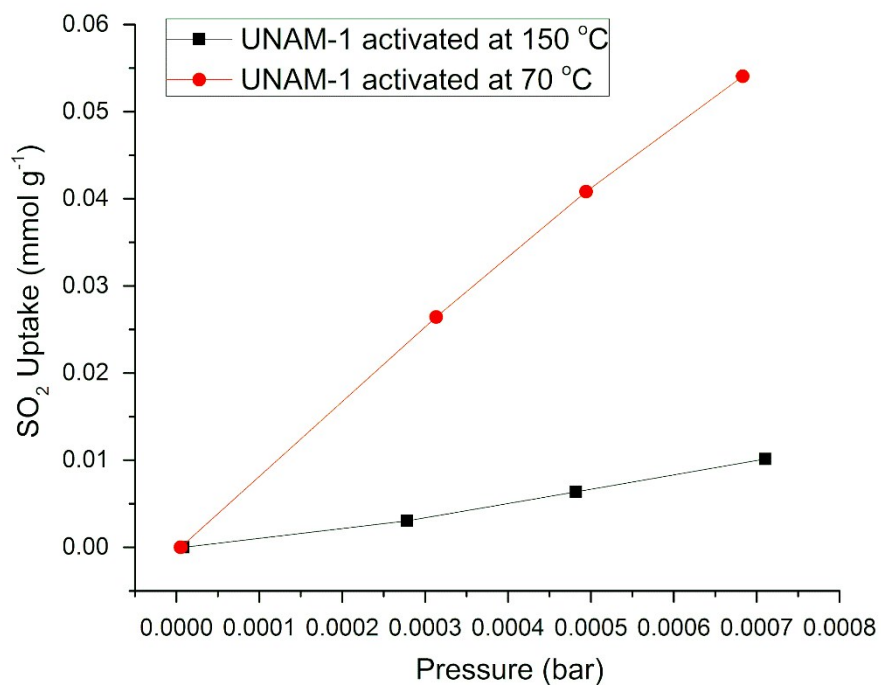**Figure S16**. SO$_2$ sorption isotherm of **UNAM-1** activated at 70 °C.

Figure S17. SO$_2$ adsorption isotherms of **UNAM-1** activated at 70 °C and 150 °C.

Isosteric Heat of Adsorption for SO_2

The isosteric heat of adsorption was estimated by fitting virial-type equation to 303 and 308 K SO_2 adsorption isotherms (Figure S21).

$$Ln\left(\frac{n}{p}\right) = A_0 + A_1 n + A_2 n^2 + \cdots$$

Eq. 1

where p is the pressure, n is the amount adsorbed and A_0, A_1, ... are the virial coefficients (A_2 and higher terms can be ignored at lower coverage values). A plot of $ln(n/p)$ versus n should give a straight line at low surface coverage (Figure S22). The heat of adsorption was estimated in –17.52 kJ mol^{-1}.
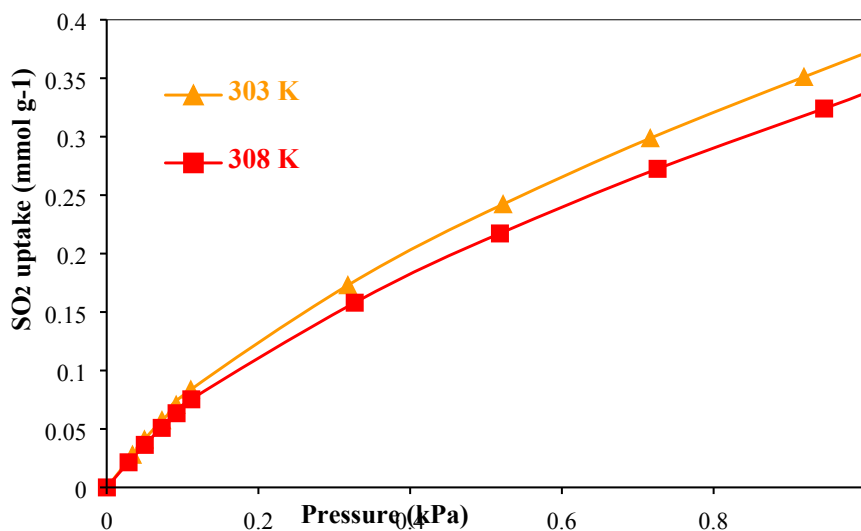
Figure S18. SO_2 adsorption isotherms of **UNAM-1** at 303 and 308 K at low pressures.
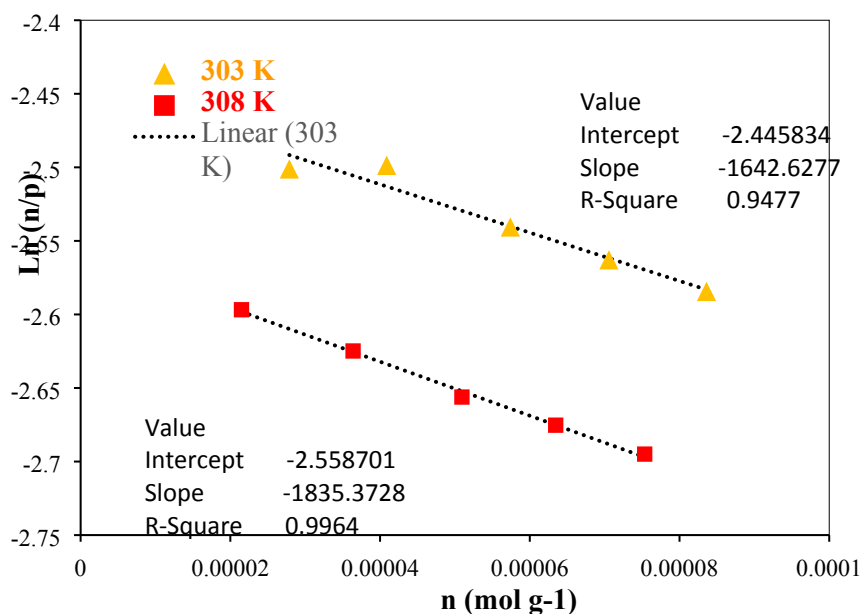
Figure S19. Virial fitting plots for adsorption of SO_2 on **UNAM-1** at 303 and 308 K.
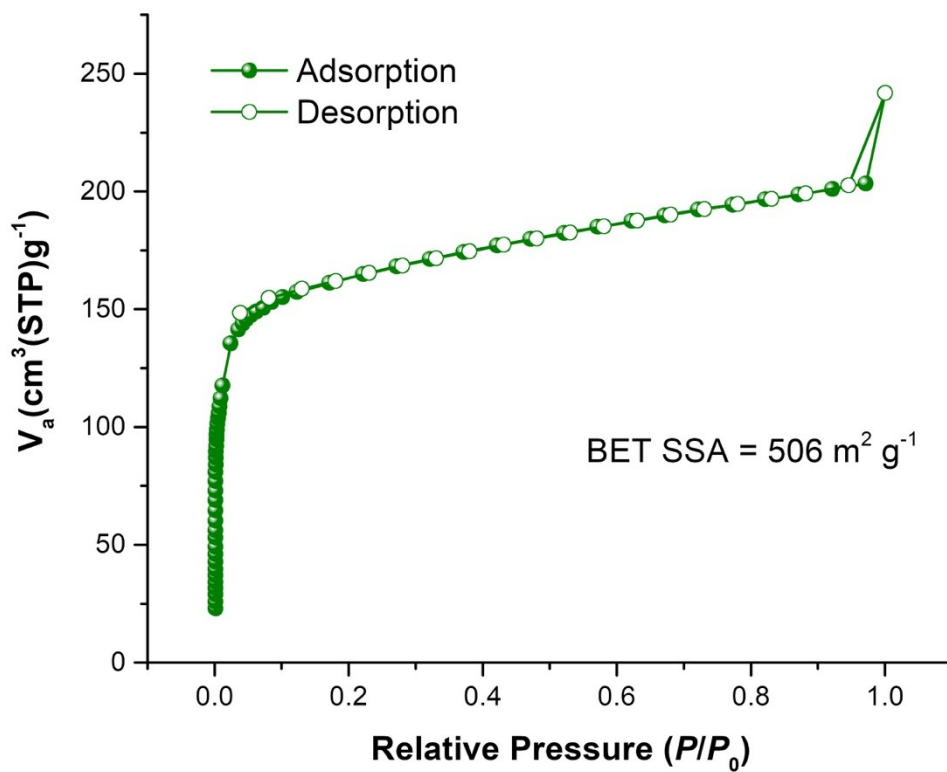
Figure S20. N_2 sorption isotherm of **UNAM-1** activated at 120 °C and collected at 77 K.
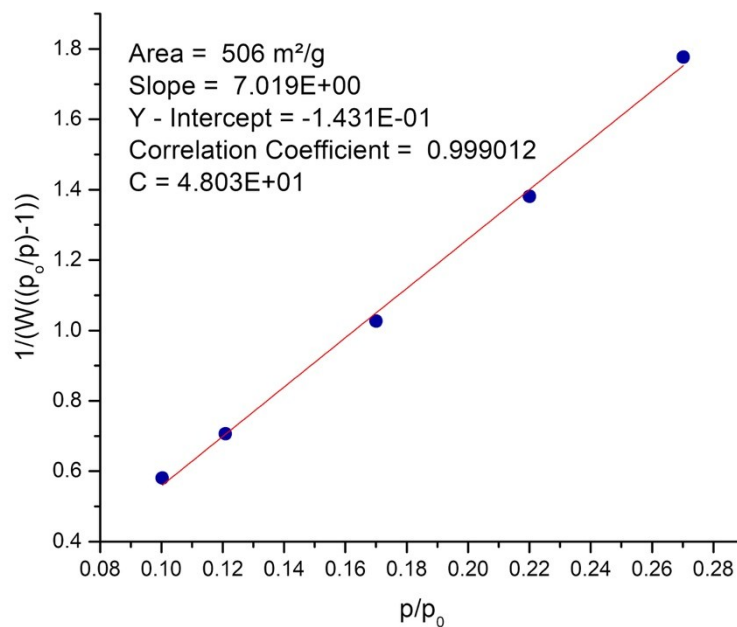
Figure S21. Plot of the linear region for the BET equation (from the N_2 adsorption isotherm of UNAM-1 activated at 120 °C).

Figure S22. Experimental SO$_2$ adsorption isotherms (at 35 ^{0}C and up to 1 bar) collected for activated **UNAM-1** at 70 ^{o}C, activated **UNAM-1** at 120 ^{o}C, hexane-solvent exchanged **UNAM-1** (activated at 70 ^{o}C) and DCM-solvent exchanged **UNAM-1** (activated at 70 ^{o}C) samples.

Table S5. Comparison of SO_2 adsorption capacity of **UNAM-1** with some MOFs.

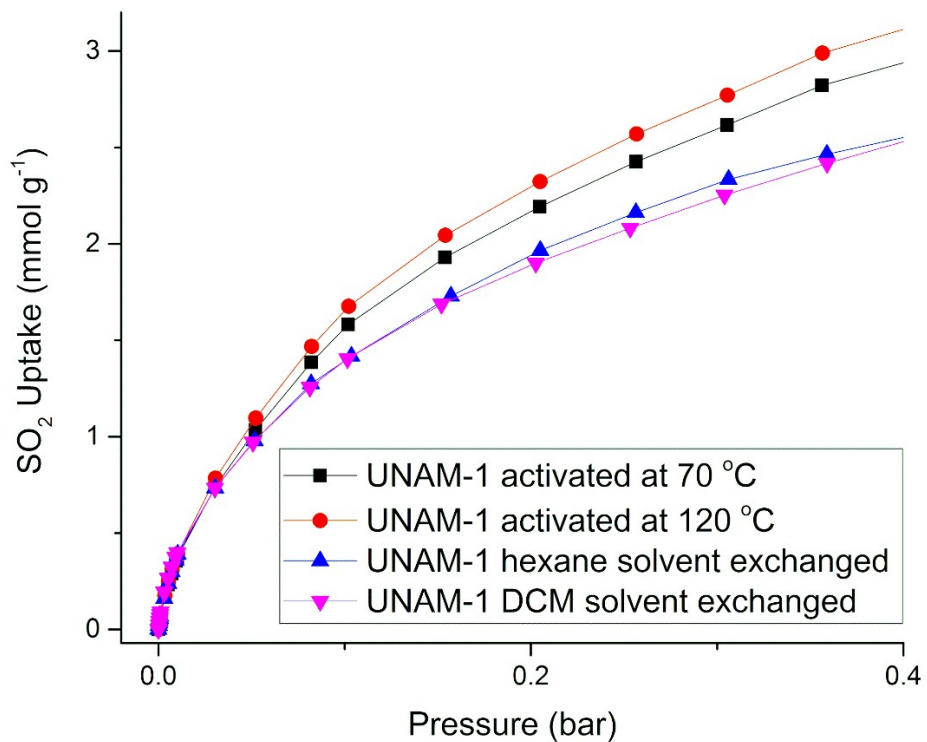| Material	S_{BET} (m$^2 \cdot$g^{-1})	SO_2 uptake (mmol$\cdot$g^{-1})	Pressure (bar)	Temperature (K)	Ref.
UNAM-1	522	3.5	1	298	This work
	522	1.58	0.1	298	
SIFSIX-3-Zn	250	2.1	1	298	11
SIFSIX-3-Ni	368	2.74	1	298	11
FMOF-2	378	1.79	Dynamic sorption	298	12
Zn-MOF-74	632	3.03	Dynamic sorption	298	13
ZnCo analogues	700	1.68	1	298	14
ELM-12	706	2.5	1	298	15
MIF zeolite	713	2.6	1	298	16
Mg-MOF-74	1206	1.56	Dynamic sorption	298	17
Zn-MOF-74	496	0.256	Dynamic sorption	298	17
MFM-305-CH$_3$	256	5.16	1	298	18
MFM-305	779	6.99	1	298	18
MIL-160	1170	4.2	0.01	293	19
CAU-10	625	4.47	1	298	-
UiO-66-ox	1410	0.8	<0.1	298	20
HKUST-1	1264	0.49	Dynamic sorption	298	13
KAUST-7	280	1.4	500 ppm of SO_2	298	21
KAUST-8	258	1.6	500 ppm of SO_2	298	21

Monte Carlo Integration

Experimental

The accessible surface areas[22, section 1.5] were calculated from a simple Monte Carlo integration technique where the probe molecule is "rolled" over the framework surface. For this, a probe molecule was randomly inserted around each of the framework atoms in turn and checked for overlap with other framework atoms. The fraction of the probe molecules that did not overlap with other framework atoms was then used to calculate the accessible surface area. The FORTRAN source code to do simulation was downloaded from the Tina Düren Research Group website.[23] The diameters of the framework atoms were taken from the UFF force field (Table S6). We use 10 000 insertions of nitrogen probe with a diameter of 3.681 Å.[24]

Table S6: Diameter of framework atoms taken as σ Lennard-Jones parameter of Universal Force Field.[25]

Atom	σ, A
H	2.571
C	3.431
N	3.261
O	3.118
Cu	3.114

The calculated geometric surface area (Table S7) is bigger than the experimental BET surface area (522 $m^2 \cdot g^{-1}$) suggesting that the pores are partially blocked by solvent molecules that did not evolve during the degassing process.

Table S7: Surface area calculated from crystal structure rolling nitrogen over framework surface.

Parameter	value
Accessible surface area	3197.24 Å^2
Accessible surface area per volume	946.97 $m^2 \cdot cm^{-3}$
Accessible surface area per mass	764.30 $m^2 \cdot g^{-1}$

References

1. G. H. Suverkropp, P. L. Alsters, C. S. Snijder and J. G. De Vries, United States Patent US005917049A, 1999.
2. *SAINT* and *SADABS*; Bruker AXS Inc.: Madison, WI, 2007.
3. G. M. Sheldrick, *Acta Cryst.*, 2015, **A71**, 3.
4. G. M. Sheldrick, *Acta Cryst.*, 2015, **C71**, 3.
5. C. B. Hübschle, G. M. Sheldrick and B. Dittrich, *J. Appl. Crystallogr.* **2011**, *44*, 1281.
6. Diamond, Copyright © 1997-2014 Crystal Impact GbR, Bonn, Germany. Author: K. Brandenburg. Version 3.2k (05-2014)
7. CorelDRAW© X7, Version 17.0.0.491. ©2014
8. Mercury CSD 2.0 - New Features for the Visualization and Investigation of Crystal Structures. C. F. Macrae, I. J. Bruno, J. A. Chisholm, P. R. Edgington, P. McCabe, E. Pidcock, L. Rodriguez-Monge, R. Taylor, J. van de Streek and P. A. Wood, *J. Appl. Cryst.* 2008, **41**, 466–470.
9. Persistence of Vision Raytracer (Version 3.6), Persistence of Vision Pty. Ltd. **2004**, http://www.povray.org

10. GIMP 2.8: The GNU Image Manipulation Program. http://www.gimp.org.

11. X. Cui, Q. Yang, L. Yang, R. Krishna, Z. Zhang, Z. Bao, H. Wu, Q. Ren, W. Zhou, B. Chen and H. Xing, *Adv. Mater.*, 2017, **29**, 1606929.

12. C. A. Fernandez, P. K. Thallapally, R. K. Motkuri, S. K. Nune, J. C. Sumrak, J. Tian and J. Liu, *Cryst. Growth Des.*, 2010, **10**, 1037.

13. D. Britt, D. Tranchemontagne and O. M. Yagui, *Proc. Natl. Acad. Sci. USA*, 2008, **105**, 11623.

14. P. K. Thallapally, R. K. Motkuri, C. A. Fernandez, B. P. McGrail and G. S. Behrooz, *Inorg. Chem*, 2010, **49**, 4909.

15. Y. Zhang, P. Zhang, W. Yu, J. Zhang, J. Huang, J. Wang, M. Xu, Q. Deng, Z. Zeng and S. Deng, *ACS Appl. Mater. Interfaces*, 2019, **11**, 10680.

16. J. Matito-Martos, A. Martin-Calvo, J. J. Gutiérrez-Sevillano, M. Haranczyk, Doblare, J. B. Parra, C. O. Ania and S. Calero, *Phys. Chem. Chem. Phys.*, 2014, **16**, 19884.

17. T. G. Glover, G. W. Peterson, B. J. Schindler, D. Britt and O. M. Yagui, *Chem. Eng. Sci.*, 2011, **66**, 163.

18. L. Li, I. da Silva, D. I. Kolokolov, X. Han, J. Li, G. Smith, Y. Cheng, L. L. Daemen, C. G. Morris, H. G. W. Godfrey, N. M. Jacques, X. Zhang, P. Manuel, M. D. Frogley, C. A. Murray, A. J. Ramirez-Cuesta, G. Cinque, C. C. Tang, A. G. Stepanov, S. Yang and M. Schröder, *Chem. Sci.*, 2019, **10**, 1472.

19. P. Brandt, A. Nuhnen, M. Lange, J. Möllmer, O. Weingart and C. Janiak, *ACS Appl. Mater. Interfaces*, 2019, **11**, 17350.

20. J. B. DeCoste, Tyler J. Demasky, M. J. Katz, O. K. Farha and J. T. Hupp, *New J. Chem.*, 2015, **39**, 2396.

21. M. R. Tchalala, P. M. Bhatt, K. N. Chappanda, S. R. Tavares, K. Adil, Y. Belmabkhout, A. Shkurenko, A. Cadiau, N. Heymans, G. De Weireld, G. Maurin, K. N. Salama and E. Eddaoudi, *Nat. Commun.*, 2019, **10**, 1328.

22. A. R. Leach. Molecular modelling: principles and applications. Prentice Hall, 2001.

23. T. Düren, F. Millange, G. Férey, K. S. Walton, R. Q. Snurr, *J. Phys. Chem. C*, 2007, **111**, 15350–15356.

24. M. V. Parkes, H. Demir, S. L. Teich-McGoldrick, D. S. Sholl, J. A. Greathouse, M. D. Allendorf, *Micropor. Mesopor. Mat.*, 2014, **194**, 190–199.

25. Web site for obtaining the source code of the program to calculate the accessible surface area. https://people.bath.ac. uk/td222/research/surface_area/index.html Accessed Oct. 24, 2019.